JOURNAL OF MATERIALS SCIENCE 26 (1991) 1078–1086

The fracture of concentrically loaded square ceramic plates

K. M. ENTWISTLE
Materials Science Centre, University of Manchester/UMIST, Grosvenor Street, Manchester, M1 7HS UK

A testing system is described which measures the fracture stress of square plates. The loading is concentric and the plate is simply supported at the corners. The effective stressed volume can conveniently be changed by varying the diameter of the loading circle. The test is used to measure the fracture characteristics of square alumina plates 103 mm square and 1 mm thick. The displacement of the centre of the plate at fracture is about 3 mm, so the elastic system is geometrically non-linear. A non-linear finite element analysis using the ABAQUS program gave a stress distribution that was found to be in very good agreement with measured stress. The finite element solution was used to calculate stress–volume and stress–area integrals, which are tabulated, and these give the effective volumes and areas, for loading circles of 25 and 7.5 mm diameter. Two batches of plates were fractured, one with a loading circle of 25 mm diameter and the other 7.5 mm. Weibull plots were made assuming zero threshold stress. The first plots used the maximum tensile stress in the plate derived from the measured load using the finite element solution. This stress occurs at the intersection of the plate diagonal with the loading circle. Different values of m (19.58 and 15.48) were given for the two loading circle diameters. Plots based on the stress determined at the fracture origin gave nearly identical values of m (13.92 and 13.72). Weibull statistics and the values of the stress–volume or the stress–area integrals were used to predict the ratio of the average fracture stress for the two loading circle diameters. The predictions showed good agreement with the measured values. The stress–area integrals, which are simpler to calculate, gave almost as good predictions as did the stress–volume integrals.

1. Introduction

A variety of loading systems has been used to measure the fracture stress of brittle materials. For uniaxial tension, three-point and four-point bend loading are popular [1] and the radial expansion of a ring [2] has merit. The diametral compression of a "θ" specimen has been proposed in an attempt, not entirely successfully, to avoid the severe experimental difficulty of securing uniform stress in a rod or strip in tension. Biaxial stress tests include diametral compression of a disc [3], called the Brazilian test, and a variety of forms of lateral loading of discs, including uniform pressure on a simply supported disc [4], central loading of a disc and "ball on ring" loading [5].

The work now described aimed to extend the range of loading systems by exploring the possibility of using concentrically loaded square plates simply supported at each corner, as a fracture test for ceramics under biaxial tension. The advantage of a test that uses square plates is that ceramic material is often fabricated in this shape. Also the maximum stress is in the central region so the edges of the plate, where the defect population is frequently atypical of the bulk of the material, is less intensely stressed and fracture is not initiated there. The use of concentric loading provides a convenient means, through changing the diameter of the loading circle, of exploring the effect on the fracture statistics of changing the volume of the stressed material. An investigation of this volume effect is reported.

A disadvantage of a test using square plates is that they are seldom perfectly flat which demands adjustment of the height of one of the corner supports. It was established that, for the 103 mm square plates of alumina used in the work now described, it was possible to correct for out-of-flatness by putting a suitable shim under the corner of the plate that did not touch the support. The thickness of the shim required was never more than 0.1 mm which is less the 1/30 of the central deflection of the plates at the point of fracture.

If one corner of the plate does not touch the corner support in the unloaded state then the relation between applied load and the strains measured at the centre of the plate shows a characteristic discontinuity at the point where the plate deflection causes the fourth corner to make contact with the support. The use of shims in the manner now described was found to eliminate this discontinuity.

For stiffer plates, with a higher ratio of thickness to diagonal length than those used in this investigation, adjustment of the corner support will be more critical.

1.1. The stresses and deflections in the loaded plate

The alumina plates were 103 mm square and about 1 mm thick. They were supported at the four corners

0022–2461/91 $03.00 + .12

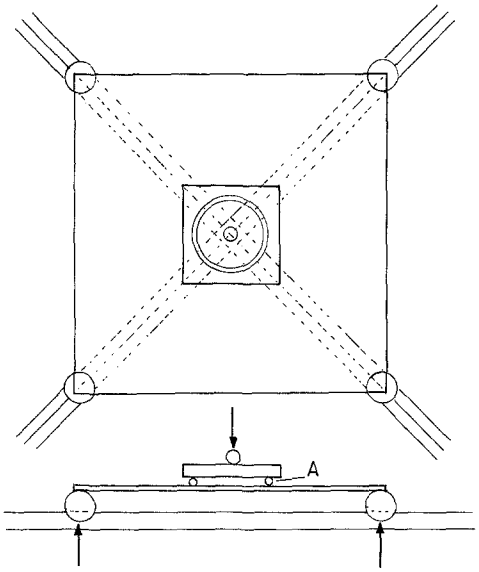

Figure 1 Diagram showing the supporting and loading arrangements for the plate. A, neoprene "O" ring.

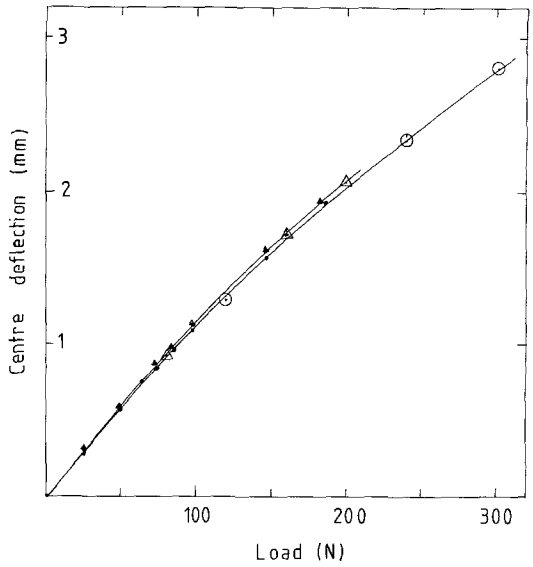

Figure 2 Relation between applied load and deflection of the plate at the centre. 25 mm loading circle; (○) finite element solution, (●) measured. 7.5 mm loading circle; (△) finite element solution, (▲) measured.

on 9.5 mm diameter steel spheres located in diagonal "V" grooves in a substantial square steel plate (Fig. 1). This arrangement permits free radial movement of the points of support as the plate deflects. The concentric load was applied through a neoprene "O" ring. Circumferential uniformity of the concentric load was secured by placing a square steel plate on top of the "O" ring and locating a 4 mm diameter steel sphere, through which the load was applied, precisely in the centre of the "O" ring.

Complex movements of the corner points of support arise as the plate deflects. There are three contributions:

(i) due to the change of slope of the plate at the point of support (maximum 0.3 mm inwards);

(ii) due to elastic strain in the underside of the plate (maximum 0.05 mm outwards);

(iii) due to shortening of the projected length of the deflected mid-plane of the plate (maximum 0.1 mm inwards).

The maximum combined effect is an inward movement of each point of support by about 0.35 mm. This in itself has a trivial effect on the relation between applied load and the stress in the plate and no correction has been made for it. There is also no danger of the plate rolling off the corner supports.

The relation between load and the central deflection of the plate was measured and is plotted in Fig. 2 for loading circles of 25 mm and 7.5 mm diameter. The relation is non-linear at displacements above about 0.6 mm. The centre deflection at the fracture loads is about 3 mm, which is about three times the plate thickness. Under these large deflections the system is geometrically non-linear, as Fig. 2 reveals, and membrane stresses arise.

It is desirable to carry out a detailed stress analysis of the loaded specimen in any fracture test, because rarely are conditions such that simple assumptions about the stress distribution are valid. In this case a finite element analysis, which took account of the non-linearity, was carried out to calculate the stress distribution in the plate as a function of applied load. This used the non-linear ABAQUS program.

The value of Young's modulus for the alumina plates, needed for this analysis, was measured by comparing the load required to produce a centre deflection of 0.25 mm, which is well within the range of linear behaviour, for an alumina plate and a steel plate of similar dimensions. Two comparisons were made, one with a loading circle 25 mm diameter and the other of 7.5 mm diameter. It was assumed that the centre deflection was proportional to $Pa^2(1 - \nu^2)/Et^3$, where P is the applied load, a is the length of the side of the square plate, t is the plate thickness, E is Young's modulus, and ν is Poisson's ratio. It was assumed that for steel $E = 207\ \mathrm{GN\,m^{-2}}$ and $\nu = 0.30$, and for alumina $\nu = 0.25$. Measurements for both loading circle diameters gave a value of $E = 360\ \mathrm{GN\,m^{-2}}$ which is the value used in the finite element analysis. The value is consistent with the observed porosity of 2.5%.

The finite element calculations were carried out for two diameters of loading circle, 25 and 7.5 mm. The finite element meshes for these two conditions are shown in Figs 3 and 4. The mesh is finer in the vicinity of the loading circle for the 7.5 mm diameter case, because the stress gradients are steeper. The applied loads were 120, 240 and 300 N for the 25 mm circle, and 80, 160 and 200 N for the 7.5 mm circle. The upper end of these load ranges corresponds to the average fracture loads for the alumina plates with the respective loading circle diameters.

The central deflection calculated by the finite element programme showed good agreement with the measured values (see Fig. 2), which indirectly confirms the accuracy of the measured value of Young's modulus for the alumina plates.

Fig. 5a and b show the radial variation of the maximum principal stress, σ_1, calculated by the finite element programme for 25 and 7.5 mm diameter loading circles at loads close to the average fracture loads

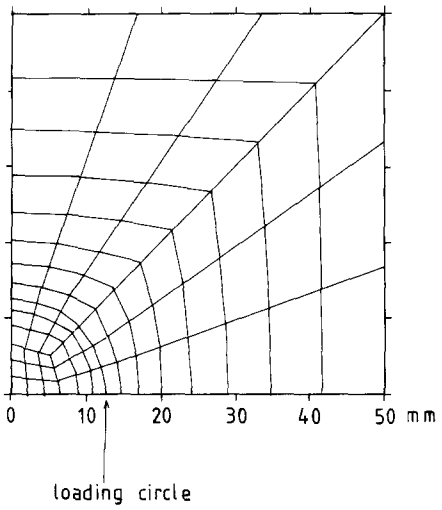

Figure 3 Finite element mesh for a 25 mm diameter loading circle.

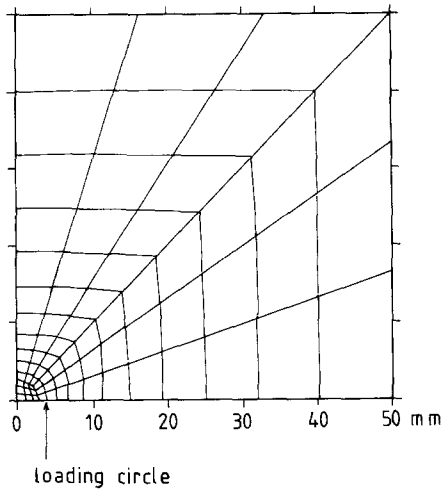

Figure 4 Finite element mesh for a 7.5 mm diameter loading circle.

of the alumina plates. The stress rises to a maximum at the load line and the increase from the centre of the plate is greater for the larger diameter loading circle. The greatest stress occurs on the loading circle where it is intersected by the plate diagonal. The stress variation within the loading circle is much less for the smaller diameter loading circle.

The stresses calculated by the ABAQUS program were compared with measured values using 0–45°–90° strain gauge rosettes, with a gauge length of 1 mm. Because the plates are so thin, corrections had to be made for the stacking geometry of the gauges. The distance of the three gauge elements from the plate surface was measured by preparing a micro-section through the rosette and photographing it at a calibrated magnification.

Fig. 6a to c compare the measured values of the tensile principal stresses, σ_1 and σ_2, on the tensile surface of the plate with the calculated values at three locations, one at the centre of the plate and the other two corresponding to the points of maximum and minimum values of σ_1 round the loading circle of 25 mm diameter. The results emphasize the non-linearity of the load–stress relations. Fig. 6a includes measured and calculated values at the centre of the plate on the compressive face and confirms that membrane stresses exist there. Fig. 7 shows a similar comparison for the stresses at the centre of the plate for a 7.5 mm diameter loading circle. The data show excellent agreement between the measured and calculated values. On the strength of this evidence the calculated stresses have been used to analyse the fracture data.

1.2. Fracture analysis

We report measurements of the fracture loads of batches of square alumina plates concentrically loaded. We explore the validity of analysing these data using Weibull statistics with zero threshold stress.

The fracture survival probability, P_s, for specimens uniformly stressed to a value σ is given by

$$P_s = \exp\left[-\left(\frac{\sigma}{\bar{\sigma}}\right)^m \left(\frac{1}{m!}\right)^m\right] \quad (1)$$

where $\bar{\sigma}$ is the average fracture stress of a batch of specimens, m is the Weibull modulus and $(1/m!)$ is the gamma function $\gamma[(1/m) + 1]$.

The fracture survival probability of an inhomogeneously stressed specimen is derived from the product of the survival probabilities of the individual

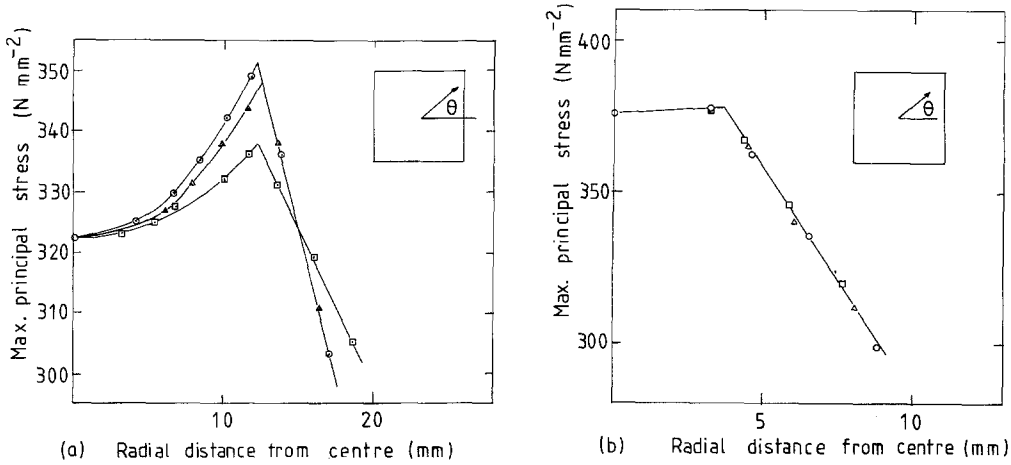

Figure 5 Variation of maximum principal stress, σ_1 with radial distance from centre for three directions (○) $\theta = 45°$, (△) $\theta = 22.5°$, (□) $\theta = 0°$. (a) 25 mm diameter loading circle. (b) 7.5 mm diameter loading circle.

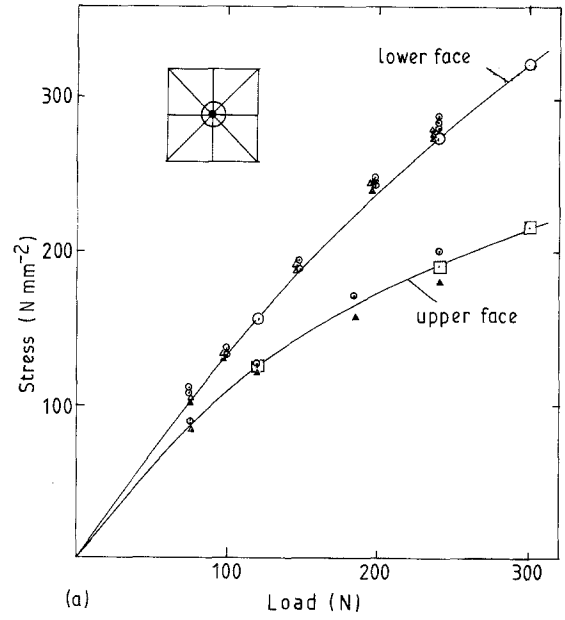

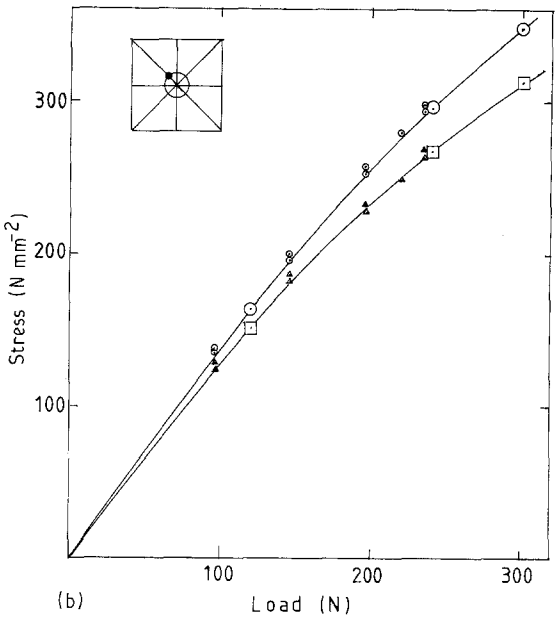

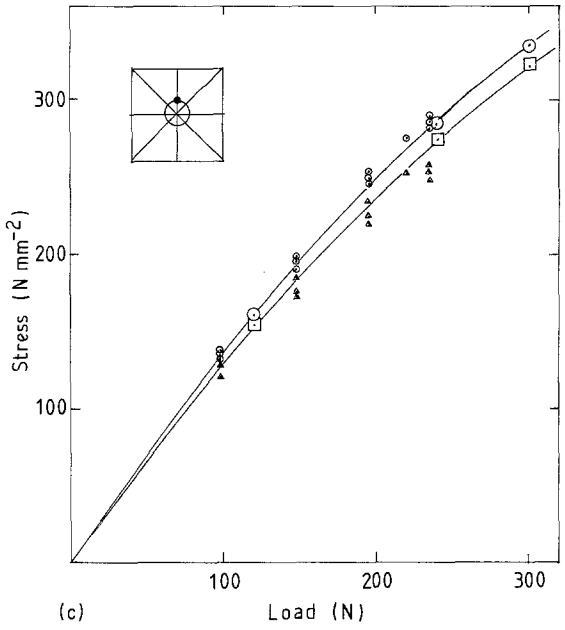

Figure 6 Comparison between the (○, △) measured and (○, □) calculated (finite element) principal stresses for a 25 mm diameter loading circle. (a) at the centre of the plate, on both upper and lower faces; (b) at the intersection between the loading circle and a plate diagonal (the point of greatest principal stress); (c) at the intersection between the loading circle and the line joining the midpoint of opposite sides of the plate. (○) σ_1, (△) σ_2, (○, □) $\sigma_1 = \sigma_2$.

elements. This approach, which implies that general fracture is initiated when the weakest element fails, predicts [6]

$$P_s = \exp\left[-\frac{1}{\bar{\sigma}_A^m}\left(\frac{1}{m}!\right)^m \sum_1^N \sigma_i^m \Delta V_i \right] \quad (2)$$

where $\bar{\sigma}_A$ is the average fracture stress of a specimen of unit volume uniformly stressed, σ_i is the maximum tensile stress in an element i of volume ΔV_i and the body comprises N elements.

The sum is made non-dimensional by introducing the total volume of the specimen, V_0, and the peak tensile stress in the whole specimen, σ_p, whence

$$P_s = \exp\left[\left(\frac{\sigma_p}{\bar{\sigma}_A}\right)^m \left(\frac{1}{m}!\right)^m K_v V_0 \right] \quad (3)$$

where

$$K_v = \sum_1^N \left(\frac{\sigma_i}{\sigma_p}\right)^m \frac{\Delta V_i}{V_0} \quad (4)$$

The effective volume, V_E, is defined as $K_v V_0$, and is the volume of an homogeneously stressed specimen which would have the same fracture survival probability at a stress σ_p as the inhomogeneously stressed specimen at a peak stress of σ_p.

The region in which fracture is initiated in the plates that are our concern is stressed in biaxial tension and both tensile principal stresses σ_1 and σ_2 contribute to the fracture probability. We take account of σ_1 and σ_2 by assuming that the overall fracture probability is the product of all the element fracture probabilities associated with both σ_1 and σ_2 acting independently. An alternative assumption has been assessed by Batdorf and Cross [7], that the fracture probability of an element depends on the macroscopic stress perpendicular to the crack plane for a uniform distribution of randomly oriented cracks. Batdorf has shown [8] that the fracture probability for a biaxially stressed element derived on this assumption is related by a constant factor, for a given value of m, to the probability computed on the assumption that σ_1 and σ_2 act independently. So the assumption of independence of σ_1 and σ_2 which we adopt herein will give the same relative values of K for different stressed volumes as does Batdorf's assumption.

It then follows that if σ_1 and σ_2 act independently

$$P_s = \exp\left[-\left(\frac{\sigma_p}{\bar{\sigma}_A}\right)^m \left(\frac{1}{m}!\right)^m K_{V2} V_0 \right] \quad (5)$$

where

$$K_{V2} = \sum_{i=1}^N \left(\frac{\sigma_{1i}^m + \sigma_{2i}^m}{\sigma_p^m}\right) \frac{\Delta V_i}{V_0} \quad (6)$$

where σ_{1i} is the greatest principal stress in element i and σ_{2i} is the lesser tensile principal stress. The effective volume of the specimen

$$V_{E2} = K_{V2} V_0 \quad (7)$$

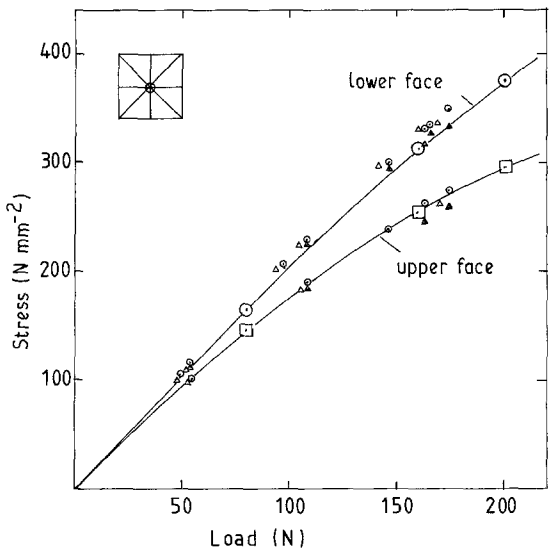

Figure 7 Comparison between the (○, △) measured and (○, □) calculated (finite element) principal stresses at the centre of the plate (both upper and lower faces). (○) σ_1, (△) σ_2, (○, □) $\sigma_1 = \sigma_2$. Loading circle diameter, 7.5 mm.

Alternatively it can be assumed that fracture is always initiated at the surface and that therefore only the surface tensile stresses contribute to the fracture probability. Under these circumstances the survival probability becomes

$$P_s = \exp\left[- \left(\frac{\sigma_p}{\bar{\sigma}_A}\right)^m \left(\frac{1}{m}!\right)^m A_0 \times \sum_1^N \left(\frac{\sigma_{1i}^m + \sigma_{2i}^m}{\sigma_p^m}\right) \frac{\Delta A_i}{A_0} \right] \quad (8)$$

where A_0 is the total area of the tensile face of the specimen and ΔA_i is the area of the ith element.

The effective area $A_{E2} = K_{A2} A_0$ where

$$K_{A2} = \sum_{i=1}^{N} \left(\frac{\sigma_{1i}^m + \sigma_{2i}^m}{\sigma_p^m}\right) \frac{\Delta A_i}{A_0} \quad (9)$$

If the average peak stress at fracture for a batch of specimens of effective volume V_{E2} is $\bar{\sigma}_{VE2}$ then, for a specimen stressed to a specific peak stress σ_p, the survival probability is

$$P_s = \exp\left[- \left(\frac{\sigma_p}{\bar{\sigma}_{VE2}}\right)^m \left(\frac{1}{m}!\right)^m \right] \quad (10)$$

This is identical to Equation 5 whence it follows that

$$\frac{K_{V2} V_0}{\bar{\sigma}_A^m} = \frac{1}{\bar{\sigma}_{VE2}^m} \quad (11)$$

but because $\bar{\sigma}_A^m$ is a constant for a particular material

$$\bar{\sigma}_{VE2}^m K_{V2} V_0 = \text{constant} \quad (12)$$

or

$$\bar{\sigma}_{VE2}^m V_{E2} = \text{constant} \quad (13)$$

So if a batch of specimens all of effective volume V'_{E2} have an average fracture stress of $\overline{\sigma'_{VE2}}$ and another batch of specimens all of effective volume V''_{E2} have an average fracture stress of $\overline{\sigma''_{VE2}}$ then the analysis predicts that

$$\overline{\sigma'_{VE2}}^m V'_{E2} = \overline{\sigma''_{VE2}}^m V''_{E2} \quad (14)$$

The corresponding relationship for surface nucleated fracture is

$$\overline{\sigma'_{AE2}}^m A'_{E2} = \overline{\sigma''_{AE2}}^m A''_{E2} \quad (15)$$

where $\overline{\sigma'_{AE2}}$ is the average peak stress at fracture of a batch of specimens all of effective area A'_{E2}.

We test the accuracy with which these expressions predict the relationship between the measured fracture stresses in the work now described.

Values of K_{V2} and K_{A2} were computed from the finite element solution for the stresses in each element and the element area or volume. The stresses were given at the four gauss points in each element.

For the calculation of K_{A2} it was assumed that the tensile surface stress at each gauss point could be assigned to a quarter of the area of the element.

The calculation of K_{V2} was based on calculated surface stresses at the four gauss points in each element on the lower (usually tensile) and upper (compressive) faces of the plate. It was assumed that each principal stress varied linearly across the plate (Fig. 8) where σ_{1i} is the surface tensile stress and σ'_{1i} is the surface compressive stress for the ith element. If t_1 is the depth of the layer stressed in tension, and t is the plate thickness then if σ_x is the value of the stress a distance x from the plane of zero stress, we require

$$\int_0^{t_1} \sigma_x^m \, dV \quad (16)$$

ignoring the contribution of compressive stresses to the fracture probability.

If the area of the element is ΔA_i then $dV = \Delta A_i dx$ and the integral becomes

$$\Delta A_i \int_0^{t_1} \left(\frac{\sigma_{1i} x}{t_1}\right)^m dx = \frac{\Delta A_i t_1 (\sigma_{1i})^m}{(m+1)} \quad (17)$$

where

$$t_1 = \frac{\sigma_{1i}}{\sigma_{1i} + \sigma'_{1i}} t \quad (18)$$

A similar expression arises from the contribution of the second tensile principal stress σ_{2i} where the depth of the tensile region

$$t_2 = \frac{\sigma_{2i}}{\sigma_{2i} + \sigma'_{2i}} t \quad (19)$$

summing these terms over all the elements, then

$$K_{V2} = \frac{1}{(m+1)} \sum_{i=1}^{N} \frac{\sigma_{1i}^m t_1 \Delta A_i + \sigma_{2i}^m t_2 \Delta A_i}{\sigma_p^m t A_0} \quad (20)$$

where A_0 is the area of the lower face of the plate. In performing these sums, if either principal stress at the gauss point on the lower face of the plate was compressive, its contribution to the fracture survival probability was assumed to be zero.

Because of the geometrical non-linearity, t_1 and t_2 vary over the plate because the magnitude of the membrane stresses vary. However, it turned out that within the region of the plate which makes the major contribution to the fracture probability, t_1 and t_2 are

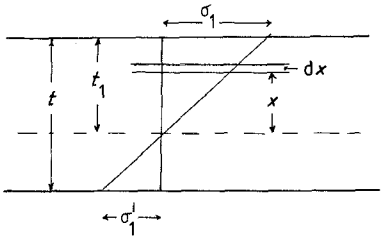

Figure 8 Diagram showing the basis for the calculation of the volume–stress integral.

constant and nearly equal. If we put $t_1 = t_2 =$ constant in Equation 20 then

$$K_{V2} = \left[\frac{t_1}{t(m+1)}\right] \sum_{i=1}^{N} \left\{\frac{\sigma_{1i}^m + \sigma_{2i}^m}{\sigma_p^m}\right\} \frac{\Delta A_i}{A_0} \quad (21)$$

or

$$K_{V2} = \frac{t_1}{t(m+1)} K_{A2} \quad (22)$$

So K_{V2} is proportional to K_{A2} and each will predict the same effect of stressed volume on the average fracture stress.

Table I lists computed values of K_{V2} and K_{A2} for loading circle diameters of 7.5 and 25 mm and loads of 200 and 300 N, respectively. These loads are close to the average fracture loads for the alumina plates. The table confirms that the ratio of the values of K_{A2} for the two loading circle diameters and the corresponding ratio of K_{V2} values are close, so Equations 14 and 15 will predict the same ratio of average fracture stresses for the two loading geometries.

Table II lists values of K_{A2} for a range of m values and for three load values for the two loading circle diameters. The K values are quite sensitive to m at low m values, as would be expected, but in the load range which produces fracture of the plates the K values are not very sensitive to load value. For $d = 25$ cm, σ_1 contributes about 80% to the total fracture probability and for $d = 7.5$ cm about 60%.

In the testing method now described, the stressed volume of the material can be varied by changing the loading circle diameter. It is of interest to establish how changes of the diameter of the loading circle are related to changes of the effective area.

The ratio of the areas within the loading circle of diameters 25 and 7.5 mm is 11.1. The linear elastic solution for the stresses in the plate shows nearly constant stress within the loading circle. For high values of m, σ^m will fall off steeply outside the loading circle, so the ratio of effective areas should approach 11.1. The non-linear case with which we are concerned is more complex. An estimate of the real effective surface area of the plate contributing to fracture is obtained by halving the values of K_{A2}, because two principal stresses are included in the computation of K_{A2}. Table III lists these values and, for comparison, the fraction of the plate surface within the loading circle, f, both for the 7.5 and 25 mm loading circles. In the case of the 7.5 mm diameter loading circle, the values of $K_{A2}/2$ approach f at high values of m but are still about $1.5f$ at $m = 20$. This is because the region outside the loading circle makes a significant contribution to fracture probability; the stress inside the loading circle is nearly constant. In contrast, for the 25 mm loading circle the values of $K_{A2}/2$ are less than f at high values of m. This is because the stresses rise from the centre of the plate to the line of the loading circle (see Fig. 5) so the major contribution to the fracture probability comes from an annular region

TABLE I Comparison of K values based on area and volume. Concentrically loaded square plates 100 mm × 1.01 mm thick supported at the corners. $E = 360\ \text{GN m}^{-2}$, $\nu = 0.25$

m	K_{A2}			K_{V2}		
	$d = 7.5$ mm, load 200 N	$d = 25$ mm load 300 N	Ratio $K_{25}/K_{7.5}$	$d = 7.5$ mm, load 200 N	$d = 25$ mm, load 300 N	Ratio $K_{25}/K_{7.5}$
10	0.020 81	0.127 40	6.12	1.045×10^{-3}	6.195×10^{-3}	5.92
13.82	0.015 45	0.077 72	5.03	5.769×10^{-4}	2.846×10^{-3}	4.93
15	0.014 54	0.068 6	4.71	5.030×10^{-4}	2.332×10^{-3}	4.63
17.53	0.013 10	0.054 27	4.14	3.913×10^{-4}	1.598×10^{-3}	4.08
20	0.012 10	0.044 69	3.69	3.189×10^{-4}	1.160×10^{-3}	3.63

TABLE II Effect of applied load and Weibull modulus, m, on the values of K_{A2}

Loading circle diameter (mm)	m	K_{A2}				
		80 N	120 N	200 N	240 N	300 N
25	10		0.132 09		0.124 78	0.127 40
	13.82		0.093 73		0.079 56	0.077 72
	15		0.086 17		0.071 11	0.068 60
	17.83		0.073 66		0.057 58	0.054 27
	20		0.064 59		0.048 23	0.044 69
7.5	10	0.023 57	0.021 80	0.020 81		
	13.82	0.017 36	0.016 27	0.015 45		
	15	0.016 33	0.015 34	0.014 54		
	17.83	0.014 72	0.013 89	0.013 10		
	20	0.013 64	0.012 90	0.012 10		

TABLE III Values of $K_{A2}/2$ compared with the fraction of the area of the plate, f, within the loading circle

m	$K_{A2}/2$		
	25 mm diameter loading circle, 300 N load	7.5 mm diameter loading circle, 200 N load	Ratio $K_{25}/K_{7.5}$
10	0.0637	0.0104	6.12
15	0.0343	0.00727	4.71
20	0.0223	0.00605	3.69
	$f = 0.0491$	$f = 0.00442$	$f_{25}/f_{7.5} = 11.11$

round the loading circle which has an area less than that within the loading circle.

The fact that, for the reasons explained, $K_{A2}/2 < f$ for $d = 25$ mm and $K_{A2}/2 > f$ for $d = 7.5$ mm means that the ratio of $(K_{A2})_{25\text{ mm}}/(K_{A2})_{7.5\text{ mm}}$ is significantly less than the ratio of the areas within the respective loading circles and decreases as m increases. So the magnitude of the size effect obtained by varying the diameter of the loading circle is less than might appear at first sight.

2. Experimental procedure

Fracture tests were carried out on 103 mm square alumina plates 1 mm thick using the concentric loading system now described. The plates are produced for the substrate for electrical circuits and were kindly donated by Vesuvius Zyalons Ltd. The advantage of this material for the purpose of the present research is that the production process incorporates an effective system of statistical control which secures a consistent structure from plate to plate. The plates are substantially pure alumina. The sintering conditions give a porosity of 2.5%. The grain size is between 2 and 10 μm.

One batch of plates was tested with a loading circle diameter, d, of 25 mm and another batch with $d = 7.5$ mm. Prior to loading to fracture the plates were heated overnight in an open stack in an oven at 150 °C. Each plate was tested immediately after it had been removed from the oven and had cooled to room temperature. The cross-head speed of the testing machine was 5 mm min^{-1}; it took a little over half a minute to fracture a plate.

Plate fracture was initiated close to the loading circle. Typical crack patterns for the 25 and 7.5 mm diameter loading circles are shown in Fig. 9. The point of greatest tensile stress lies on the loading line at the intersection with a plate diagonal. Fracture was not always initiated at that point because of statistical variations of flaw size. The location of the fracture origin for all the plates in the two batches was determined.

3. Analysis of experimental data

For the two batches of plates a Weibull plot was made of $\ln\ln(1/P_s)$ against $\ln\sigma_f$, where σ_f is the fracture stress of the plate, and the survival probability $P_s = (n/N + 1)$. The rank order fracture stress of the plate is n and N is the total number of specimens in the batch. In the plot in Fig. 10, σ_f is the maximum tensile stress in the plate at fracture. This stress arises at the point of intersection of the loading circle and the plate diagonal and was determined from the fracture load using the finite element results. The Weibull moduli, m, were determined from a least squares fit of a straight line through the experimental points expressed as $\ln\ln(1/P_s)$ and $\ln\sigma_f$, respectively.

The mean fracture stress and the value of m is given in Table IV for loading circles of 25 and 7.5 mm diameter. The specimens with the larger stressed volume have the lower average fracture stress, so a size

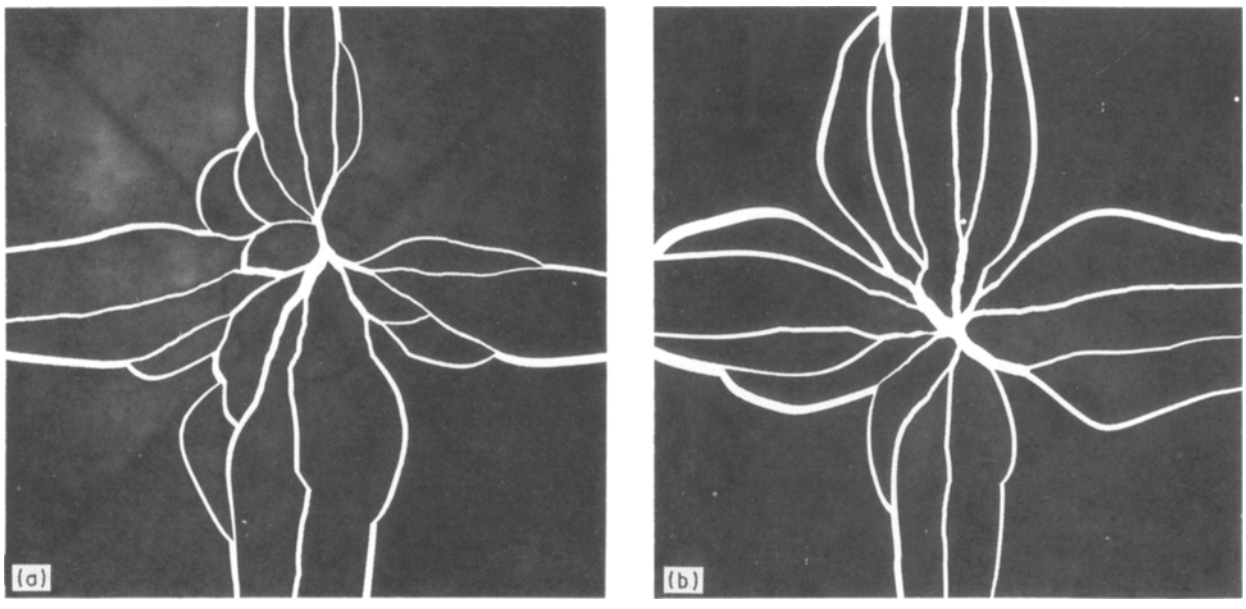

Figure 9 Typical crack patterns for fractured plates: (a) 25 mm diameter loading circle; (b) 7.5 mm diameter loading circle. The fracture origins are close to the loading circle in each case.

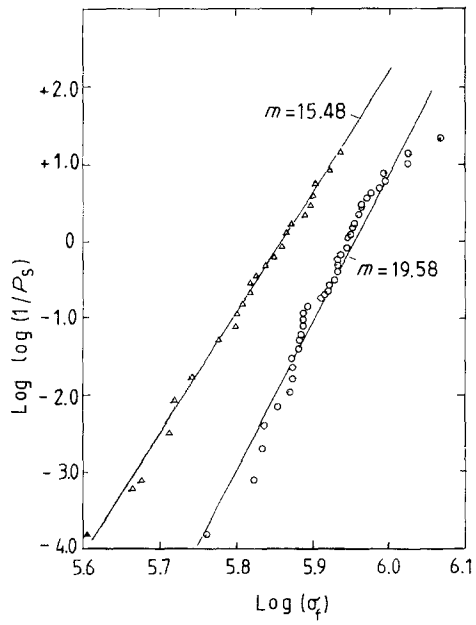

Figure 10 Weibull plots of fracture stress-survival probability for two batches of alumina plates: (○) loading circle 7.5 mm diameter; (△) loading circle 25 mm diameter. The fracture stress, σ_f, here is the maximum tensile principal stress in the specimen which occurs at the point of intersection of the loading circle and a plate diagonal on the lower face of the plate.

TABLE IV Fracture data for alumina plates

Loading circle diameter (mm)	Mean fracture stress (N mm^{-2})	Weibull modulus, m	K_{A2} for $m = 17.53$
7.5	375.1	19.58	0.013 10
25	340.6	15.48	0.054 27

effect is established. The values of m are comparable but not equal.

We now compare the relationship between the average fracture stresses for the two loading circle diameters with that predicted from Weibull statistics. Because the two batches of plates are of identical size, A_0 is the same for each, so it follows from Equation 15 that

$$\bar{\sigma}_{7.5}^{m}(K_{A2})_{7.5} = \bar{\sigma}_{25}^{m}(K_{A2})_{25} \quad (23)$$

where $\bar{\sigma}_{7.5}$ is the average fracture stress for the batch of plates fractured with a 7.5 mm diameter loading circle. For the comparison we use the average value of m, 17.53, and the values of K_{A2} for this are given in Table IV. The data yield

$$\left(\frac{\bar{\sigma}_{7.5}}{\bar{\sigma}_{25}}\right)^{m} = 5.43 \quad (24)$$

$$\frac{(K_{A2})_{25}}{(K_{A2})_{7.5}} = 4.14 \quad (25)$$

According to Weibull statistics these ratios should be equal.

The agreement is quite good. To illustrate this, if we accept that the average fracture stress for $d = 25$ mm is 340.6 N mm^{-2}, the Weibull statistics predict that

$$\bar{\sigma}_{7.5} = 340.6(4.14)^{1/17.53} = 369.4 \text{ N mm}^{-2} \quad (26)$$

This compares with the measured value of 375.1 N mm^{-2}. The error in the prediction is about 16% of the difference between the two average fracture stresses.

An alternative analysis was prompted by the observation that the fracture origins were not always located at the point of maximum tensile stress in the plate. The stress at the head of a larger flaw in a region of lower nominal stress may be higher than that at the head of a smaller flaw at the point of greatest nominal stress. In this situation the fracture origin is displaced from the point of maximum stress. The origin of fracture was located in each plate and the tensile principal stresses at that location were determined from the stress distribution calculated by the finite element analysis. The Weibull plots in Fig. 11 use fracture stresses determined by this procedure. The fracture data are gathered in Table V.

Again, making the Weibull comparison using the average of the two m values,

$$\left(\frac{\bar{\sigma}_{7.5}}{\bar{\sigma}_{25}}\right)^{13.82} = 4.39 \quad (27)$$

$$\frac{(K_{A2})_{25}}{(K_{A2})_{7.5}} = 5.03 \quad (28)$$

The ratio of K_{A2} values predicts that, if the measured fracture stress for $d = 25$ mm is 328.4 N mm^{-2}, then that for $d = 7.5$ should be 369.1 N mm^{-2} compared with the measured value of 365.5 N mm^{-2}. The error in this prediction is about 10% of the difference between the two measured values, which is better than the previous comparison.

The values of K_{V2} are listed in Table V. If we use these effective volume values to predict the relationship between the average fracture stresses we get, referring to Equation 15,

$$\frac{(K_{V2})_{25}}{(K_{V2})_{7.5}} = 4.93 = \left(\frac{\bar{\sigma}_{7.5}}{\bar{\sigma}_{25}}\right)^{m} \quad (29)$$

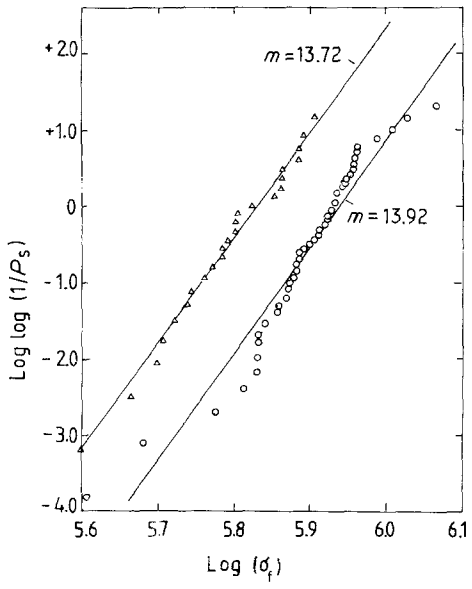

Figure 11 Weibull plots of the same data as in Fig. 10 but here σ_f is the maximum tensile principal stress at the location of the fracture origin for each plate. (○) 7.5 mm diameter, (△) 25 mm diameter.

TABLE V Fracture data for alumina plates based on fracture stresses calculated at the fracture origin

Loading circle diameter (mm)	Mean fracture stress (N mm^{-2})	m	K_{A2} for $m = 13.82$	K_{V2} for $m = 13.82$
7.5	365.5	13.92	0.01545	2.846×10^{-3}
25	328.4	13.72	0.07772	5.76×10^{-4}

This predicts a value of 368.6 N mm^{-2} for the average fracture stress for $d = 7.5$ mm. The error is 8.4% of the measured difference, which is slightly less than that for the prediction based on effective areas.

4. Discussion

A test using concentrically loaded square plates simply supported at the corners is shown to be a valid method for measuring the fracture characteristics of brittle materials. It has been demonstrated that the test can also measure stress–volume effects conveniently.

It has been shown that, if the Weibull analysis uses the maximum stress in the plate at fracture for the fracture stress, then the Weibull modulus varies with the stressed volume. This raises a fundamental question about the validity of the use of Weibull statistics to analyse such data. The reason for the variation of m values is that an element of the statistics is the scatter in the value of $(\sigma_p - \sigma_f)$ where σ_p is the maximum stress in the specimens and σ_f is the stress at the location of the fracture origin. The effect of this is seen to be, from the results now described, to reduce the spread of fracture stress values (that is to increase m) by an amount that is greater, the smaller is the stressed volume. The magnitude of this effect will be influenced by the steepness of the stress gradients in the specimen.

The fact that the m values obtained using computed stresses at the origin of fracture are nearly equal implies that the two loading systems see a statistically significant defect population. The equality of m values also permits Weibull statistics to be used with a clearer conscience. So the use of fracture-origin stresses commends itself as a sounder basis for the prediction of stress–volume effects because it eliminates the contribution to fracture statistics from the dispersion of $(\sigma_p - \sigma_f)$ values and, in consequence, delivers data that are more closely related to material properties rather than the characteristics of a particular loading system.

The two ways explored here of presenting the fracture data each have a role. The engineer's primary interest will be in the load which the plate can carry. The statistical description of that quantity is best indicated by expressing the fracture stress as the peak stress in the plate at fracture. On the other hand, the material scientist interested in the behaviour of the material, would gain a clearer insight into the material characteristics from data based on the stress at the point of fracture initiation.

It has been demonstrated that, for these concentrically loaded square plates, prediction of the effect of stressed volume on average fracture stress can be made with similar accuracy using either effective volumes or effective areas. Because the latter are more easily computed there is a natural preference to use them.

The plates used in this research have a high ratio of diagonal length to thickness. This causes the deformation to be geometrically non-linear. For plates with lower ratios the behaviour up to fracture will be more nearly linear, but, for small ratios, shear stresses will need to be taken into account. We are exploring the stress distribution in plates of different aspect ratio and are also using the test now described to obtain fracture information on other brittle materials.

Acknowledgements

The author thanks Dr Dong Mei Qi, Department of Civil and Structural Engineering, UMIST, for her help with the finite element calculations, and Professor M. Burdekin for making the resources of that Department available. He also thanks Mr David Hutchinson for help and advice on mechanical testing techniques, and Vesuvius Zyalons Ltd for the supply of alumina plates.

References

1. H. FESSLER and D. C. FRICKER, *J. Strain Anal.* **19** (1984) 197.
2. R. SEDLACEK and F. HALVEN, *Rev. Sci. Instrum.* **33** (1962) 298.
3. M. C. SHAW, P. M. BRAIDEN and G. J. de SALVO, *Trans. AIME J. Eng. Ind.* **97** (1975) 77.
4. D. A. GORHAM and D. G. RICKERBY, *J. Phys. E.* **8** (1975) 794.
5. D. K. SHETTY, A. R. ROSENFIELD, P. McGUIRE, G. J. BANSAL and W. H. DUCKWORTH, *Amer. Ceram. Soc. Bull.* **59** (1980) 1193.
6. P. STANLEY, H. FESSLER and A. D. SIVILLE, *Proc. Brit. Ceram. Soc.* **22** (1973) 453.
7. S. B. BATDORF and J. G. CROSS, *Trans. AIME J. Appl. Mech.* **41** (1974) 459.
8. S. B. BATDORF, *Int. J. Fract.* **13** (1977) 5.

Received 23 February
and accepted 9 March 1990